

June 2, 2022

An *HST* View of the Interstellar Environments of Young Stellar Objects in the Large Magellanic Cloud

Kaushar Vaidya, You-Hua Chu, Robert A. Gruendl

Department of Astronomy, University of Illinois at Urbana-Champaign, 1002 West Green Street, Urbana, IL 61801, USA

C.-H. Rosie Chen

Department of Astronomy, University of Virginia, 530 McCormick Road, Charlottesville, VA 22904, USA

and

Leslie W. Looney

Department of Astronomy, University of Illinois at Urbana-Champaign, 1002 West Green Street, Urbana, IL 61801, USA

ABSTRACT

We have used archival *HST* $H\alpha$ images to study the immediate environments of massive and intermediate-mass young stellar object (YSO) candidates in the Large Magellanic Cloud (LMC). The sample of YSO candidates, taken from Gruendl & Chu (2009), was selected based on *Spitzer* IRAC and MIPS observations of the entire LMC and complementary ground-based optical and near-infrared observations. We found *HST* $H\alpha$ images for 99 YSO candidates in the LMC, of which 82 appear to be genuine YSOs. More than 95% of the YSOs are found to be associated with molecular clouds. YSOs are seen in three different kinds of environments in the $H\alpha$ images: in dark clouds, inside or on the tip of bright-rimmed dust pillars, and in small H II regions. Comparisons of spectral energy distributions for YSOs in these three different kinds of environments suggest that YSOs in dark clouds are the youngest, YSOs with small H II regions are the most evolved, and YSOs in bright-rimmed dust pillars span a range of intermediate evolutionary stages. This rough evolutionary sequence is substantiated by the presence of silicate absorption features in the *Spitzer* IRS spectra of some YSOs

in dark clouds and in bright-rimmed dust pillars, but not those of YSOs in small H II regions. We present a discussion on triggered star formation for YSOs in bright-rimmed dust pillars or in dark clouds adjacent to H II regions. As many as 50% of the YSOs are resolved into multiple sources in high-resolution *HST* images. This illustrates the importance of using high-resolution images to probe the true nature and physical properties of YSOs in the LMC.

Subject headings: H II regions — Magellanic Clouds — stars: formation

1. Introduction

The *Spitzer Space Telescope*, with its high angular resolution and sensitivity at mid-infrared wavelengths, has made it possible for the first time to survey massive young stellar objects (YSOs) in nearby external galaxies. In particular, in the Large Magellanic Cloud (LMC), because of its close proximity (50 kpc; Feast 1999) and low inclination ($\sim 30^\circ$; Nikolaev et al. 2004), massive and intermediate-mass YSOs can be resolved by *Spitzer* and inventoried throughout the entire galaxy. The LMC was observed by *Spitzer* under a Legacy Program, Surveying the Agents of Galaxy Evolution (SAGE), that mapped the central $7^\circ \times 7^\circ$ area of the galaxy (Meixner et al. 2006). Gruendl & Chu (2009) made use of the archival *Spitzer* data from the SAGE survey along with complementary ground-based optical and near-infrared observations and identified a comprehensive sample of massive and intermediate-mass YSO candidates of the entire LMC. This sample consists of a total 855 *definite*, 317 *probable*, and 213 *possible* massive ($> 10 M_\odot$) and intermediate-mass ($> 4 M_\odot$) YSO candidates. Most of these YSO candidates are found to be concentrated in or around molecular clouds or H II regions (Gruendl & Chu 2009).

While *Spitzer* enables the detection of individual massive and intermediate-mass YSOs in the LMC (e.g., Chu et al. 2005; Jones et al. 2005; Caulet et al. 2008; Whitney et al. 2008; Gruendl & Chu 2009), the angular resolution of *Spitzer* is not sufficient to resolve multiple sources within 1–2'' or allow a close look at the environments of these massive YSOs. The *Hubble Space Telescope (HST)* on the other hand, with an angular resolution ten times higher than that of *Spitzer*, reveals sub-arcsec size features and hence is very useful for a detailed examination of the environments of these massive YSOs.

We have therefore searched through the *HST* archive for continuum and H α images that cover LMC YSO candidates from the above catalog. In many cases, the exposure times of the continuum images are short and hence not very useful, as noted by Chen et al. (2009). The H α images have longer exposure times and are very useful in revealing

interstellar environments of YSOs in H II complexes where the interstellar gas is photoionized by antecedent massive stars. For example, ionization fronts on the surface of dense molecular clouds can be recognized by the sharply enhanced $H\alpha$ surface brightness. $H\alpha$ images are also useful in revealing circumstellar environments of massive YSOs. For example, the UV flux of a YSO may photoionize its circumstellar medium and form a compact H II region, or outflows from a YSO may produce observable features like Herbig-Haro objects (Heydari-Malayeri et al. 1999; Chu et al. 2005). Thus, in this paper we make use of primarily the *HST* $H\alpha$ images to examine the immediate surroundings of the LMC YSO candidates. The continuum images are only used to supplement the analyses of stellar properties for a few YSOs.

The remaining paper is organized as follows: Section 2 describes the datasets used in this work and our method of analysis, Section 3 describes the environments of YSO candidates, Section 4 discusses the properties of small H II regions discovered around some massive YSO candidates, Section 5 describes the mid-infrared spectral characteristics of some YSO candidates, Section 6 discusses the spectral energy distributions (SEDs) of the YSO candidates, Section 7 presents a discussion on triggered star formation, and finally Section 8 summarizes the paper.

2. Datasets and Method of Analysis

We searched the *HST* archive for $H\alpha$ images observed with the Wide Field Planetary Camera 2 (WFPC2) and the Advanced Camera for Surveys (ACS) for a field of ~ 78 degree² centered on the LMC coordinates ($\alpha = 05^h 18^m$, $\delta = -68^\circ 34'$), available as of 2008 August. WFPC2 consists of four cameras, PC1, WF2, WF3, and WF4, among which PC1 has a field-of-view of $36'' \times 36''$ with a scale of $0''.045$ pixel⁻¹, and the remaining three cameras each have a field-of-view of $80'' \times 80''$ with a scale of $0''.1$ pixel⁻¹ (McMaster et al. 2008). The ACS observations were made in the Wide Field Channel (WFC), which has a field-of-view of $202'' \times 202''$ with a scale of $0''.05$ pixel⁻¹ (Boffi et al. 2007). The $H\alpha$ filters F656N ($\lambda_c = 6564\text{\AA}$, $\Delta\lambda = 22\text{\AA}$) and F658N ($\lambda_c = 6584\text{\AA}$, $\Delta\lambda = 72\text{\AA}$) were used with WFPC2 and ACS observations, respectively.

As noted in Gruendl & Chu (2009), we have been imaging YSO candidates in selected regions throughout the LMC in the near-infrared J and K_s bands with the IR Side Port Imager (ISPI) on the Blanco 4 m telescope at the Cerro Tololo Inter-American Observatory. The ISPI camera has a $10'.25 \times 10'.25$ field-of-view imaged with a 2048×2048 HgCdTe Array with $0'.3$ pixels. In total, we have imaged 113 fields in four different runs, 2005 November, 2006 November, 2007 February, and 2008 January. During our last run in 2008

January, we specifically imaged 29 fields that encompassed the *HST* archival data used in our study of YSO candidates in the LMC. These observations give us additional confirmation on the nature of the YSO candidates, bridging the gap between optical and mid-infrared wavelengths. Each field was imaged with a sequence of exposures with a telescope offset of $\sim 1'$ between frames to aid in removal of bad pixels and to facilitate sky subtraction and flat fielding. For the *J*-band observations, thirteen 30 s exposures were obtained, while at *K_s* band, twenty-three 30 s frames (each consisting of two coadded 15 s exposures) were obtained. The observations were non-linearity corrected, sky subtracted, and flat fielded using standard routines within the CIRED and SQUIID packages in IRAF. The astrometry was performed using the WCSTOOLS task IMWCS and the Two Micron All Sky Survey Point Source Catalog (2MASS PSC; Skrutskie et al. 2006). In these ISPI images, we find that point sources with $m_J \lesssim 18.5$ and $m_K \lesssim 17.6$ mag are generally detected with better than $10\text{-}\sigma$ significance.

Following the method of Gruendl & Chu (2009) for assessing the nature of YSO candidates, we simultaneously displayed “postage stamp” images of each YSO candidate (field-of-view $5' \times 5'$) in the following wavelengths: Digitized Sky Survey red continuum, *HST* $\text{H}\alpha$, ISPI *J* and *K_s* bands, *Spitzer* IRAC 3.6, 4.5, 5.8, and 8.0 μm , and MIPS 24 and 70 μm , along with the SED of the YSO candidate. To examine the large-scale environments, we also used the $\text{H}\alpha$ images from the Magellanic Cloud Emission Line Survey (MCELS; Smith et al. 1999). By examining the source morphology and environment of each YSO candidate in the multiwavelength images, in conjunction with its SED profile, we conclude that 82 of the 99 YSO candidates are most likely genuine YSOs. Our evaluation of the YSO nature of the sources is consistent with the previous assessment of Gruendl & Chu (2009), as they categorized the 82 confirmed YSO candidates as *definite* YSOs and the remaining 17 YSO candidates as *probable* or *possible* YSOs, where *probable* YSOs are likely to be YSOs but also show some characteristic of a possible alternative nature, and *possible* YSOs are more likely to be non-YSOs but cannot be ruled out as YSOs. In our analysis, the majority of these 17 non-YSOs appear to be either peaks of diffuse emission or background galaxies (see the table of non-YSOs in the appendix). In the following discussion, we include only these 82 YSO candidates and refer to them as YSOs.

3. Environments of YSOs

The *HST* $\text{H}\alpha$ images provide an unprecedented detailed view of the immediate environments of YSOs in the LMC. It is remarkable that all 82 YSOs are found in only three kinds of environments: (1) in a dark cloud, (2) inside or on the tip of a bright-rimmed dust pillar,

and (3) in a small H II region. Eight YSOs are found in more than one kind of environment, e.g., a small H II region located inside a bright-rimmed dust pillar. All YSOs are illustrated by $20'' \times 20''$ ($5.0 \text{ pc} \times 5.0 \text{ pc}$) images presented in Figure 1. We also show the SEDs of YSOs in Fig. 1. For YSOs with neighboring sources within $1''$, the identification of their optical counterparts in the *HST* images is not straightforward because of the combined uncertainties in astrometry, and it is necessary to bootstrap through images at intermediate wavelengths. Therefore, in Fig. 1 we have included ISPI J and K_s , and IRAC $3.6 \mu\text{m}$ images, in addition to the *HST* $\text{H}\alpha$ images. The IRAC $3.6 \mu\text{m}$ images show the YSOs as well as a small number of background stars. The alignment between the IRAC and ISPI images can be fine-tuned with these background stars, and a YSO’s near-infrared counterpart can be identified by its being brighter in K_s than J compared with normal stars. The larger number of background stars in J makes it easier to align the ISPI images with the *HST* $\text{H}\alpha$ image and identify a YSO’s optical counterpart. General remarks of these three categories are given below.

Dark Clouds – 49 YSOs are found to be associated with dark clouds. Among these, 34 show no detectable optical counterparts and 15 show faint optical counterparts in *HST* $\text{H}\alpha$ images; their images presented in Fig. 1 are labeled as categories 1a, and 1b, respectively. It can be seen that these YSOs are in highly dusty environments, with dust features extending over several parsecs and sometimes tens of parsecs. Some YSOs are located near ionization fronts, as indicated by bright $\text{H}\alpha$ emission on the surface of dark clouds. Note that diffuse ionized gas sometimes exists along the line of sight, and in these cases dark clouds can be diagnosed only in images larger than those shown in Fig. 1, viewed with adjustable contrast. Two examples are the YSO J051351.51-672721.9 and YSO J053838.45-690418.3.

Bright-Rimmed Dust Pillars – 19 YSOs are associated with bright-rimmed dust pillars, of which eight are also associated with either dark clouds or small H II regions. These YSOs are labeled as category 2 in Fig. 1. A great majority of these YSOs are projected near the tips of bright rims of dust pillars; only three YSOs are projected inside dust pillars. The bright-rimmed dust pillars show different morphologies and sizes, but all of them are pointing toward nearby OB associations, the source of ionizing radiation. Three of the YSOs associated with dust pillars are also found to be in compact H II regions.

H II Regions – Among the 22 YSOs in this category, the existence of small H II regions ranges from “obviously seen” to “implied by generalization,” as discussed in detail later in Section 4. Briefly, eight YSOs are surrounded by resolved H II regions of sizes up to $7''.5$ ($\sim 1.8 \text{ pc}$); four YSOs appear more extended than the point spread function (PSF) in the *HST* $\text{H}\alpha$ images, suggesting the existence of barely resolved H II regions; four YSOs have observed fluxes in the $\text{H}\alpha$ band higher than the expected stellar continuum fluxes, indicating excess $\text{H}\alpha$ emission from ionized circumstellar gas; the remaining six YSOs either do not show

significant excess H α emission or have no optical photometric data to assess the expected continuum fluxes. The images of YSOs with well-resolved, barely resolved, and unresolved H II regions shown in Fig. 1, are labeled as categories 3a, 3b, and 3c, respectively.

To examine the molecular environment of these YSOs, we have compared the locations of YSOs with the NANTEN CO (J=1–0) survey of the LMC, made with a 4-m telescope for a beamsize of 2'6 (Fukui et al. 2001, 2008). We find that 70 YSOs are superposed on giant molecular clouds detected by NANTEN. The remaining 12 YSOs might be associated with small pc-sized molecular clouds with masses lower than a few $\times 10^4 M_{\odot}$, the NANTEN detection limit. The high-resolution *HST* H α images show that indeed 7 of these are in a visibly dusty environment. These results indicate that at least 95% of the 82 YSOs we examined are still associated with molecular material.

In Table 1 we summarize the YSOs and their properties: column 1 is the running number; column 2 lists the identifier of the YSOs from Gruendl & Chu (2009); column 3 describes the environment derived from *HST* H α images; columns 4 and 5 give the names of the associated H II region from Davies et al. (1976) and Henize (1956), respectively; column 6 lists whether the YSO is associated with molecular clouds detected by the NANTEN survey (Fukui et al. 2001); column 7 lists nearby OB associations (Lucke & Hodge 1970); columns 8 and 9 are described in §5; and the last column is described in §6. In some cases YSOs are found in more than one kind of environment, e.g., YSOs which are surrounded by small H II regions and are also associated with bright-rimmed dust pillars. For such YSOs, column 3 indicates both the environments. There are also some cases where more than one YSO is discovered in the *Spitzer* PSF. Such cases are indicated in column 3 as well.

4. Properties of H II Regions

Of the 82 YSOs, 22 show small ionized regions that are well resolved, marginally resolved, or unresolved by the *HST* PSF (FWHM $\sim 0'.1$). For H II regions with different degrees of resolution, different methods are needed to measure the H α fluxes from the *HST* images and to assess whether the unresolved sources possess H α line emission.

Resolved H II Regions– For the eight YSOs that show well resolved H II regions, we measured the H α fluxes of the H II regions using the *HST* images, following the procedures for narrow-band WFPC2 photometry¹. Images were divided by the exposure time and then the count rates were multiplied by the PHOTFLAM parameter found in the image headers to

¹Available at http://www.stsci.edu/instruments/wfpc2/wfpc2_faq/wfpc2_nrw_phot_faq.html

get flux densities. To obtain the fluxes, we multiplied the flux densities with the rectangular filter width calculated with SYNPHOT to be 28.3Å and 74.9Å for the filters F656N and F658N, respectively.

To remove the stellar continuum from the integrated H α flux of a well-resolved H II region, we simply excised point sources from the H α image and replaced them with the average of the surrounding diffuse emission, as most of the H II regions do not have broadband continuum images available. One YSO in a resolved H II region, YSO J052207.27-675819.7, has continuum images in the F675W band. Using the F675W image and the H α image, we estimate that the stellar continuum contributes $\sim 17\%$ of the total observed H α flux within the boundary of the H II region, while using the H α image alone we find the stellar flux contributes $\sim 14\%$ of the total flux. These results suggest that excising point sources from the H α images is adequate for continuum subtraction. The continuum-subtracted H α fluxes of the H II regions are listed in Table 2.

Assuming an electron temperature of 10^4 K, the H α surface brightness (SB) of an H II region can be expressed as

$$SB = 1.9 \times 10^{-18} EM \text{ ergs s}^{-1} \text{ cm}^{-2} \text{ arcsec}^{-2},$$

where $EM \equiv n_e^2 L_{pc}$ is the emission measure of the H II region; n_e is the rms electron density in cm^{-3} , and L_{pc} is the emitting path length in parsecs. We measured the surface brightness of the H II regions directly from the images. The variations in surface brightness over these small H II regions are not significantly large. The peak brightnesses of the H II regions are typically higher by a factor of 1.2–1.5 as compared to the average brightnesses of the H II regions. We used the average value of the surface brightness and determined the emission measure of each H II region using the above relation. From the emission measure and the average size of the H II region (which we used as the average emitting path length of these H II regions), we then determined the rms electron density of the H II region. We also calculated extinction-uncorrected H α luminosities from the H α fluxes, and the required ionizing powers $Q(\text{H}^0)$ of the H II regions for their H α luminosities. Finally, we assessed the corresponding spectral types for the massive YSOs using the theoretical ionizing powers provided by Panagia (1973). Table 2 lists the observed and derived properties of all the resolved H II regions. Note that the H α luminosities, ionizing powers, and the spectral types given in Table 2 are lower limits to these quantities, as we have not applied an extinction correction.

Marginally Resolved H II Regions – There are four YSOs that show marginally resolved H II regions. We did not find *UBV* photometry for any of these four YSOs in the Magellanic Cloud Photometric Survey (MCPS; Zaritsky et al. 2004). We searched for

broad-band continuum WFPC2 and ACS images in the *HST* archive, and found useful images for two YSOs, J052212.24-675813.1, and J053838.36-690630.4. For J052212.24-675813.1, we found a continuum image in the wide-band filter F675W, and measured the continuum flux of the YSO. Scaling it according to the bandwidth, we find the expected continuum flux in the H α band to contribute only 25% of the total flux measured. The excess H α emission confirms the existence of a small H II region. For the other YSO, J053838.36-690630.4, we found the continuum images in the wide-band filters F555W and F814W. We measured the fluxes of the YSO in these two bands and interpolated between them to make a rough estimate of its expected continuum flux in the H α band. The estimated continuum flux is $\sim 21\%$ of the observed flux in the H α band. This excess H α emission also confirms the existence of a small H II region. The H α fluxes of these two marginally resolved H II regions (see Table 3) suggest that the central stars are early-type B stars, but cooler and less powerful than the earliest B stars seen in the resolved H II regions in Table 2. It is likely that the other two YSOs with extended image but no photometric data are also in small H II regions, which need to be confirmed by spectroscopic observations in the future.

Unresolved H II Regions – There are 10 YSOs that are unresolved in the *HST* H α images, but it can be deduced from photometric analysis that they exhibit excess H α emission indicating the existence of unresolved H II regions. No useful *HST* continuum images are available for these YSOs, but we found MCPS *UBV* photometry for seven of them and used these data to estimate expected stellar continuum fluxes in the H α band. We began by assuming $(B - V)_0 \sim -0.3$, the color of O and early B main sequence stars, which have ionizing powers. Adopting the canonical extinction relation $A_V \sim 3.2E(B - V)$, $E(U - B)/E(B - V) = 0.72$ for early-type stars, and a distance modulus of 18.5, we calculated their absolute magnitudes in *UBV* and the intrinsic color $(U - B)_0$, and compared these results with standard stars (Schmidt-Kaler 1982) to determine the main sequence spectral types of the YSOs. This approach works well, and we can usually narrow down the classification to within 1–2 subtypes. Using the stellar effective temperatures implied by the spectral types, we then calculated the expected (blackbody) continuum fluxes of the YSOs in the H α passband in the WFPC2 F656N or ACS F658N filter using the *calphot* task in the SYNPHOT package.

For four YSOs, J045651.82-663133.0, J053549.28-660133.5, J053609.54-691805.5, and J054853.64-700320.2, their expected continuum fluxes in the H α passband are only 10–76% of their observed H α fluxes. If we take into account the stellar photospheric absorption at the H α line, the expected stellar fluxes are even lower in the H α passband. Given that the equivalent widths of the H α absorption in early-B stars range from $\sim 3.5 \text{ \AA}$ in B0 stars to $\sim 5 \text{ \AA}$ in B2 stars (Didelon 1982), or 10–17% for the 28.3 \AA width of the F656N filter passband, we are confident that these 4 YSOs indeed have small H II regions that are not resolved by

the $0''.1$ PSF of WFPC2.

For three YSOs, J045720.72-662814.4, J053855.56-690426.5, and J053858.42-690434.7, the observed $H\alpha$ fluxes are comparable to or somewhat lower than their expected continuum fluxes in the $H\alpha$ passband. Considering the stellar photospheric absorption of the $H\alpha$ line and the fact that the observed $H\alpha$ fluxes were not extinction-corrected, it is likely that these three YSOs also have some excess $H\alpha$ emission and small unresolved H II regions. The existence of unresolved H II regions for J045720.72-662814.4 and J053858.42-690434.7 is further supported by the presence of IR spectral features that originate from ionized and partially ionized gas, as discussed later in Section 5. For the remaining three YSOs, J045429.42-690936.9, J053821.10-690617.2, and J054844.29-700360.0, we did not find existing *UBV* photometry or any *HST* broad-band images to estimate the continuum contribution in the $H\alpha$ passband; hence, we cannot determine whether these three YSOs have H II regions. Based on the results of the other seven YSOs, we consider it likely that these three YSOs also have unresolved H II regions. Table 3 lists the observed $H\alpha$ fluxes and the expected continuum fluxes in the $H\alpha$ passband of these ten YSOs with unresolved H II regions.

Finally, we note that 10–18% of B stars are known to be emission-line B stars (Jaschek & Jaschek 1983), and that we are not able to distinguish emission-line B stars from unresolved H II regions. It is nevertheless certain that stellar emission lines are formed in extended regions exterior to the photospheres, and thus the distinction may be a matter of semantics.

5. YSOs with *Spitzer* IRS Spectra

Seale et al. (2009) presented *Spitzer* Infrared Spectrograph (IRS) spectra for 277 YSO candidates selected from the Gruendl & Chu (2009) YSO catalog. They found that the IRS spectra of massive YSO candidates can be divided into six different groups based on their spectral characteristics. They proposed that these different groups reflect different evolutionary stages of massive YSOs. The groups were defined as: spectra with silicate absorption, S group; spectra with silicate absorption and fine-structure lines, SE group; spectra showing Polycyclic Aromatic Hydrocarbons (PAH) emissions, P group; spectra showing both PAH emission and fine-structure lines, PE group, spectra showing fine-structure lines, E group; and finally spectra that appear to be featureless though they may show one or more of the above characteristics, F group. Seale et al. (2009) noted that there were five YSOs in their sample which they did not classify as the spectra for these five YSOs did not have full spectral coverage. These 5 YSOs showed fine-structure lines in the IRS spectra and were termed as “embedded objects with unknown classification” by Seale et al. (2009). Many of their P and PE group YSOs showed silicate absorption features at $10\ \mu\text{m}$.

Thirty-three of our YSOs with *HST* images have *Spitzer* IRS spectra reported by Seale et al. (2009). Columns 8 and 9 in Table 1 list the classification by Seale et al. (2009) of these YSOs based on the *Spitzer* IRS spectra, and whether or not silicate absorption features are present in the IRS spectra, respectively. The YSOs which were called as “embedded objects with unknown classification” are marked as “Unknown” in Table 1. Eighteen YSOs in dark clouds have spectra, of which 14 are classified as PE or P group (where 9 of them show silicate absorption features), 2 are classified into the SE group, 1 is classified into the F group, and 1 is “embedded object with unknown classification”. Six YSOs in bright-rimmed globules have IRS spectra, of which, three are PE (with two of them in dark clouds showing silicate absorption features), one in a dark cloud is SE, and one is an “Embedded object with unknown classification”. Among the 10 YSOs whose H II regions are confirmed morphologically or photometrically, seven have IRS spectral type PE (none with silicate features) and three are “Embedded object with unknown classification”. Finally, two YSOs whose H II regions are not confirmed either morphologically or photometrically, have IRS spectral type PE (no silicate absorption features) indicating that they have small unresolved H II regions.

All the 12 YSOs with small H II regions show fine-structure lines in the spectra with 9 YSOs also showing PAH emission features. This is understandable, as fine-structure lines are expected to be present in H II regions of massive YSOs, whereas PAH emission features are generated in photodissociation regions on the surface of H II regions. Many YSOs associated with dark clouds and bright-rimmed dust pillars also show PAH emission and/or fine-structure lines which implies that these YSOs might also have ionized regions surrounding them though not seen in the *HST* H α images. It is interesting to note that none of the YSOs with small H II regions show silicate absorption features, whereas half of the YSOs in dark clouds and one-third YSOs in bright-rimmed dust pillars show silicate absorption features in the IRS spectra. Also, two YSOs in dark clouds, one of which is associated with a bright-rimmed dust pillar have been classified into the SE group—proposed by Seale et al. (2009) to be the less evolved stage compared to the P or PE group. These results suggest that the YSOs in dark clouds and in bright rimmed dust pillars are less evolved compared to YSOs with small H II regions.

6. YSO Categories and SEDs

It is highly interesting that all the LMC YSOs for which we found archival *HST* data, are found in only one of three different kinds of environments. Do the SEDs of these YSOs reflect any signatures that are characteristic of their environments? To check that, we examined

the SEDs (optical to mid-infrared) of the YSOs and searched for any possible correlation between the YSO environments and their SEDs. We first classified YSOs according to the empirical “Type” classification based on the SEDs of massive YSOs, proposed by Chen et al. (2009). In this scheme, Type I has an SED that rises steeply from near-infrared to 24 μm and beyond, Type II has an SED with a low peak at optical wavelengths and a high peak at 8–24 μm , and Type III shows an SED with bright optical peak and modest near- and mid-infrared peak (see Fig. 7 in Chen et al. 2009).

We could classify 62 of our 82 YSOs using the above SED criteria (see the last column in Table 1). For the remaining YSOs, a classification could not be made either because there are multiple sources in the near-infrared data and/or in the *HST* data within the *Spitzer* PSF, making the YSO identification difficult, or the SED does not fit into any of the above Types, e.g., YSOs that are not detected in available optical data, and are faint or not detected at 24 μm . Figure 2 shows the distribution of YSOs of different environments (column 3 in Table 1) into the Type I, II, and III classification (last column in Table 1). For many YSOs, unambiguous classification into Type II or Type III was not possible; such cases are grouped as II/III.

A correlation can be seen between YSO environments and their SEDs. YSOs in dark clouds with no optical counterparts are largely classified as Type I. YSOs in dark clouds but with optical counterparts are mostly classified as Type II. YSOs in bright-rimmed dust pillars are classified as either Type II or classification is ambiguous between II and III. YSOs with resolved H II regions are mostly classified as Type III, and YSOs with marginally resolved or unresolved H II regions are classified as Type II/III or Type III. Thus, we see that YSOs in different environments are in different evolutionary stages. YSOs in dark clouds are the youngest, YSOs with H II regions are the most evolved, and YSOs in bright-rimmed dust pillars are in the intermediate stage. Even among the YSOs in dark clouds, one can see a marked difference between the YSOs with and without optical counterparts. The YSOs with optical counterparts are more evolved as compared to YSOs without optical counterparts. The YSOs with marginally resolved and unresolved H II regions are a mix of Type II and Type III, as opposed to YSOs with resolved H II regions which are mostly Type III. This might mean that YSOs with marginally resolved and unresolved H II regions are more likely to be younger compared to YSOs with resolved H II regions.

We examined the *HST* $\text{H}\alpha$ images of YSOs to check for multiplicity. As many as 50% YSOs show multiple sources within $2''$ of the YSO location in the high-resolution *HST* images, of which 12% show multiple YSOs. In the remaining cases, the other sources are normal stars. Many of the multiples are also well resolved in the ISPI *J* and *K_s*-bands. As has been cautioned by Chen et al. (2009), multiplicity is a problem in interpreting the nature of LMC

YSOs using only *Spitzer* data. While the Chen et al. (2009) study is based only on one H II complex, N44, the current study covers a wide range of star formation environments in the LMC and demonstrates that multiplicity is indeed a prevailing problem.

7. Triggered Star Formation

The formation of massive stars has a significant impact on the structure and evolution of the interstellar medium. After their birth, massive stars radiatively ionize their ambient medium and mechanically energize their surroundings via fast stellar winds and supernova ejecta. While such energy feedback may disperse the natal molecular cloud and terminate the star formation eventually, the initial pressure increase in the ionization front on molecular material may actually trigger star formation. Using *HST* H α images, we were able to examine the relationship between YSOs and ionization fronts of antecedent massive stars.

Bright-rimmed dust pillars are potential sites of triggered star formation caused by compression due to ionization/shock fronts. One fourth of our sample, 19 YSOs, are found to be associated with bright-rimmed dust pillars. One of these YSOs is found in a dark cloud with an optical counterpart (2/1b) and four are found in dark clouds with no optical counterparts (2/1a), indicative of their youth. Three bright-rimmed dust pillars show marginally resolved small H II regions and harbor massive YSOs. In order to assess whether the star formation was induced by external pressure in these bright-rimmed dust pillars, we calculated thermal pressures of the ionized rims of the dust pillars, and present a few examples here.

YSO J045659.85–662425.9 is associated with a bright-rimmed dust pillar that shows the brightest ionized rims in all of our sample. The peak H α surface brightness of the ionized gas enveloping this dust pillar is 2.5×10^{-12} ergs s $^{-1}$ cm $^{-2}$ arcsec $^{-2}$, corresponding to an emission measure of 1.31×10^6 cm $^{-6}$ pc, for a temperature of 10^4 K. We adopt the average of the projected emission length of ~ 0.55 pc and width of ~ 0.18 pc (measured from H α image) as the emission path length, 0.36 pc, and derive a rms electron density of 1900 cm $^{-3}$. The thermal pressure of the ionized rim of the dust globule is $P/k \sim 1.9 \times 10^7$ cm $^{-3}$ K. The thermal pressure of the dust globule is $P/k \sim 10^4$ cm $^{-3}$ K, assuming typical values of density, 10^3 H $_2$ cm $^{-3}$, and temperature, 10 K, for Bok globules. The pressure of the ionized surface of the pillar is thus much higher than the thermal pressure of the dust globule, suggesting that star formation was possibly triggered by the external pressure. On another extreme, the YSO J045641.23–663132.9 is associated with a bright-rimmed dust pillar that shows the faintest rim among those in our sample. For this case, the peak H α surface brightness of the ionized gas enveloping the dust pillar is 3.7×10^{-14} ergs s $^{-1}$ cm $^{-2}$ arcsec $^{-2}$, implying an emission measure of 1.95×10^4 cm $^{-6}$ pc. The projected emission length and width on

the surface of dust pillar are 0.8 and 0.6 pc, respectively, as measured from the $H\alpha$ image. Using the average of these two values as the emission length along the line of sight, we derive a rms electron density of $\sim 170 \text{ cm}^{-3}$, and the thermal pressure of the rim $P/k \sim 1.7 \times 10^6 \text{ cm}^{-3} \text{ K}$. This is still much higher compared to the typical thermal pressure of dust globules and could also be a case of triggered star formation. We therefore conclude that most of our YSOs in the bright-rimmed dust pillars have likely formed as a result of triggering due to external pressure.

Apart from the YSOs in the bright-rimmed dust pillars, there are 2 YSOs in dark clouds in juxtaposition with H II regions, which may also represent triggered star formation. One of these two YSOs, J053630.81-691817.2, is resolved into a stellar source and a small bright H II region separated by $\sim 0''.9$ in the *HST* $H\alpha$ image. The H II region contains an unresolved point source near its peak emission, indicating that the star might be its ionizing source. The ISPI J and K_s images also show two corresponding sources, with the YSO being redder than the source in the H II region. The close proximity between the H II region and the YSO, projected distance ~ 0.2 pc, suggests that the expansion of the H II region may have compressed the molecular cloud and triggered the formation of the YSO. Another such example is presented by the YSO J045625.99-663155.5, which is projected at ~ 1 pc from a resolved small H II region, and is also a possible case of triggered star formation. The high-resolution *HST* images are indeed very useful to examine the large scale star formation environments in detail, and a systematic study of this nature is important to address issues related to formation of massive stars and the interplay of massive stars with the interstellar medium.

8. Summary

We have used archival *HST* $H\alpha$ images to examine the immediate environments of massive and intermediate-mass YSO candidates of the LMC. In total, archival *HST* $H\alpha$ images were found for 99 YSO candidates. By examining the source morphology and the environment of YSO candidates in multiwavelength images, we conclude that 82 of the candidates are genuine YSOs. All of these 82 YSOs are found in only three different environments, in dark clouds, in bright rimmed dust pillars, or in small H II regions. Forty-nine YSOs are in dark clouds, 34 of which show no optical counterparts, and the remaining 15 show faint optical counterparts in *HST* $H\alpha$ images. Nineteen YSOs are associated with bright-rimmed dust pillars, of which five are in dark clouds, and three show small H II regions. Twenty two YSOs show small H II regions, of which 8 are well resolved, 4 are marginally resolved, and the remaining 10 are unresolved in the *HST* $H\alpha$ images. We calculate observed (reddened)

H α fluxes of the resolved H II regions and present the estimated spectral types of these massive YSOs. For the marginally resolved as well as the unresolved H II regions, we use *UBV* photometry or *HST* continuum images to estimate the stellar continuum fluxes in the H α passband, and demonstrate that most of them possess H α line emission, indicating that they indeed have small H II regions.

YSOs for which *Spitzer* IRS spectra are available, predominantly show PAH emission and/or fine-structure lines in the spectra. Nine YSOs associated with dark clouds, with two of them also in bright-rimmed dust pillars, show silicate absorption features in the IRS spectra, whereas none of the YSOs associated with small H II regions show silicate absorption features. YSOs in small H II regions including the marginally resolved, and the unresolved ones, show PAH emission and/or fine-structure lines in the IRS spectra. The comparison of YSO environments with the SEDs reveal an evolutionary sequence of YSOs in different environments. YSOs in dark clouds with no optical counterparts are mostly Type I and hence the youngest. YSOs in dark clouds but with optical counterparts are mostly Type II and more evolved compared to YSOs with no optical counterparts. YSOs in bright-rimmed dust pillars are either Type II or Type II/III and are in the intermediate stage. YSOs with resolved H II regions are mostly Type III and are the most evolved. Finally, YSOs with marginally resolved H II regions, and unresolved H II regions are a mix of Type II and Type III, and should be on average younger compared to YSOs with resolved H II regions. As many as 50% YSOs are resolved into multiple sources when seen in *HST* images, signifying the importance of using high-resolution images to probe the true nature of YSOs and to study their immediate environments.

We investigate the issue of triggered star formation for YSOs in bright-rimmed dust pillars and YSOs in dark clouds adjacent to H II regions. The thermal pressures of ionized surfaces of bright-rimmed dust pillars are found to be much higher compared to typical thermal pressures of dust globules. Thus the YSOs in bright-rimmed dust pillars have likely formed due to triggering from external pressure. Finally, we show that by examining the immediate environments of the YSOs using the high-resolution *HST* images, we can learn about the evolutionary stages of massive YSOs. A systematic survey of massive YSOs using *HST* will be very useful to study the evolutionary aspects of massive YSOs and to understand star formation in wide range of interstellar environments.

This work was supported through NASA grants HST-AR-10942.01-A, JPL 1290956, and JPL 1316421. This work made use of the data products of the Two Micron All Sky Survey (2MASS), which is a joint project of the University of Massachusetts and the Infrared Processing and Analysis Center/California Institute of Technology, funded by the National Aeronautics and the Space Administration and the National Science Foundation.

REFERENCES

- Boffi, F. R. et al. 2007, ACS Instrument Handbook, Version 8.0
- Caulet, A., Gruendl, R. A., & Chu, Y.-H. 2008, *ApJ*, 678, 200
- Chen, C.-H. R., Chu, Y.-H., Gruendl, R. A., Gordon, K. D., & Heitsch, F. 2009, *ApJ*, 695, 511
- Chu, Y.-H., et al. 2005, *ApJ*, 634L, 189
- Davies, R. D., Elliott, K. H., & Meaburn, J. 1976, *MmRAS*, 81, 89
- Didelon, P. 1982, *A&AS*, 50, 199
- Feast, M. W. 1999, in IAU Symp. 190, in *New Views of the Magellanic Clouds*, ed. Y.-H. Chu, N. Suntzeff, J. Hesser, & D. Bohlender, 542
- Franco, J., Kurtz, S. E., García-Segura, G., & Hofner, P. 2000, *Ap&SS*, 272, 169
- Fukui, Y., Mizuno, N., Yamaguchi, R., Mizuno, A., & Onishi, T. 2001, *PASJ.*, 53, L41
- Fukui, Y., et al. 2008, *ApJS*, 178, 56
- Gruendl, R. & Chu, Y.-H. 2009, *ApJS*, 184, 172
- Lucke, P. B., & Hodge, P. W. 1970, *AJ*, 75, 171
- Henize, K. G. 1956, *ApJS*, 2, 315
- Heydari-Malayeri, M., Rosa, M. R., Charmandaris, V., Deharveng, L., & Zinnecker, H. 1999, *A&A*, 352, 665
- Jaschek, M., & Jaschek, C. 1983, *A&A*, 117, 357
- Jones, T. J., Woodward, C. E., Boyer, M. L., Gehrz, R. D., & Polomski, E. 2005, *ApJ*, 620, 731
- McMaster, B. et al. 2008, *WFPC2 Instrument, Handbook, Version 10.0*
- Meixner, M., et al. 2006, *AJ*, 132, 2268
- Nikolaev, S., Drake, A. J., Keller, S. C., Cook, K. H., Dalal, N., Griest, K., Welch, D. L., & Kanbur, S. M. 2004, *ApJ*, 601, 260
- Panagia, N. 1973, *AJ*, 78, 929

- Schmidt-Kaler, Th. 1982, *Physical Parameters of the Stars*, Landolt-Börnstein Numerical Data and Functional Relationships in Science and Technology, New Series, Group VI, Volume 2b, Springer-Verlag, Berlin
- Seale, J. P., Looney, L. W., Chu, Y.-H., Gruendl, R. A., Brandl, B., Chen, C.-H. R., Brandner, W., & Blake, G. A. 2009, *ApJ*, 699, 150
- Skrutskie, M. F., et al. 2006, *AJ*, 131, 1163
- Smith, R. C., & The MCELS Team 1999, in *IAU Symp.190: New Views of the Magellanic Clouds*, ed. Y.-H. Chu, N. Suntzeff, J. Hesser, & D. Bohlender, 28
- Rieke, G. et al. 2004, *ApJS*, 154, 25
- Fazio, G. G. et al. 2004, *ApJS*, 154, 10
- Whitney, B. A., et al. 2008, *AJ*, 136, 18
- Zaritsky, D., Harris, J., Thompson, I. B., & Grebel, E. K. 2004, *AJ*, 128, 1606

Table 1. Properties of YSOs with *HST* H α Images

Number	ID ^a	Category ^b	H II Region	H II Region	CO detection	OB Association	IRS Spectra	Silicate Absorption	YSO Type
YSOs in Dark Clouds									
1	J045625.99-663155.5	1a+1a*	DEM34	N11F	Yes	LH9	PE	No	I
2	J045629.02-663159.3	1a	DEM34	N11F	Yes	LH9	PE	No	II
3	J045640.79-663230.5	1a	DEM34	N11F	Yes	LH9	F	No	I
4	J045742.00-662634.4	1a	DEM34	N11C	Yes	LH13	PE	No	I
5	J045747.68-662816.9	1a	DEM34	N11D	Yes	LH13	PE	Yes	I
6	J052207.32-675826.8	1a	DEM152	N44C	Yes	LH47	–	–	I
7	J052211.86-675818.1	1a	DEM152	N44C	Yes	LH47	–	–	I
8	J052212.57-675832.4	1a	DEM152	N44C	Yes	LH47	SE	Yes	I
9	J053628.51-691636.6	1a	DEM263	N157	No	–	–	–	I
10	J053822.43-690644.4	1a	DEM263	N157	Yes	–	–	–	I
11	J053833.09-690611.9	1a	DEM263	N157	Yes	LH100	–	–	I
12	J053834.06-690452.2	1a	DEM263	N157	Yes	LH100	–	–	I
13	J053834.60-690557.0	1a	DEM263	N157	Yes	LH100	–	–	I
14	J053843.52-690629.0	1a+1b*	DEM263	N157	Yes	LH100	–	–	I
15	J053844.32-690329.9	1a+1b*	DEM263	N157	Yes	LH100	–	–	II
16	J053848.17-690411.7	1a	DEM263	N157	Yes	LH100	–	–	I
17	J053848.42-690441.6	1a	DEM263	N157	Yes	LH100	–	–	I
18	J053849.27-690444.4	1a	DEM263	N157	Yes	LH100	PE	Yes	I
19	J053852.67-690437.5	1a	DEM263	N157	Yes	LH100	PE	No	II/III
20	J053909.08-693005.7	1a	DEM269	N158C	Yes	LH101	–	–	I
21	J053912.79-693041.8	1a	DEM269	N158C	Yes	LH101	–	–	I
22	J053922.74-693011.7	1a	DEM269	N158C	Yes	LH101	–	–	II
23	J053938.73-693904.3	1a	DEM284	N160D	Yes	LH103	PE	Yes	I
24	J053943.60-693820.4	1a	DEM284	N160A	Yes	LH103	–	–	–
25	J053944.33-693847.5	1a+1b+1b*	DEM284	N160A	Yes	LH103	–	–	–
26	J054003.49-694355.0	1a	DEM271	N159D	Yes	LH105	–	–	–
27	J054009.49-694453.5	1a	DEM271	N159B	Yes	LH105	PE	Yes	I
28	J054019.01-694445.6	1a	DEM271	N159G	Yes	LH105	–	–	–
29	J054839.05-700536.4	1a	DEM323	N180B	Yes	LH117	–	–	–
30	J045627.37-663201.0	1b	DEM34	N11F	Yes	LH9	–	–	II
31	J045633.02-662359.8	1b	DEM34	N11B	Yes	LH10	–	–	–
32	J045638.76-662446.2	1b	DEM34	N11B	Yes	LH10	PE	No	I
33	J045725.75-662545.8	1b	DEM34	N11	Yes	–	–	–	II
34	J051351.51-672721.9	1b	DEM106	N30B	No	LH38	P	Yes	II/III
35	J052208.52-675922.1	1b	DEM152	N44C	Yes	LH47	–	–	II
36	J053630.81-691817.2	1b	DEM263	N157	No	–	P	No	II
37	J053838.45-690418.3	1b	DEM263	N157	Yes	LH100	–	–	II
38	J053904.88-692949.9	1b	DEM269	N158C	Yes	LH101	PE	No	II
39	J053906.31-693043.8	1b	DEM269	N158C	Yes	LH101	PE	Yes	II
YSOs in Bright-Rimmed Dust Pillars									

Table 1—Continued

Number	ID ^a	Category ^b	H II Region	H II Region	CO detection	OB Association	IRS Spectra	Silicate Absorption	YSO Type
40	J045628.68-663143.4	2/1b [†]	DEM34	N11F	Yes	LH9	–	–	II
41	J045641.23-663132.9	2	DEM34	N11F	Yes	LH9	–	–	II
42	J045657.25-662513.0	2/1a [†]	DEM34	N11B	Yes	LH10	–	–	II/III
43	J045659.85-662425.9	2	DEM34	N11B	Yes	LH10	PE	No	III
44	J045737.61-662726.7	2	DEM34	N11C	Yes	LH13	–	–	III
45	J045739.04-662731.3	2	DEM34	N11C	Yes	LH13	–	–	–
46	J051829.16-691458.1	2	DEM132A	N119	No	LH41	–	–	II/III
47	J052135.83-675443.0	2	DEM152A	N44F	Yes	LH47	–	–	–
48	J052601.20-673012.1	2/1a [†]	DEM192	N51D	No	LH54	SE	Yes	–
49	J052619.79-673033.6	2	DEM192	N51D	No	LH54	–	–	–
50	J053609.54-691805.5	2/3c [†]	DEM263	N157	No	–	–	–	II/III
51	J053623.52-691002.1	2	DEM263	N157	No	–	–	–	II/III
52	J053838.36-690630.4	2/3b [†]	DEM263	N157	Yes	LH100	–	–	III
53	J053839.23-690552.2	2	DEM263	N157	Yes	LH100	PE	No	II
54	J053839.69-690538.2	2/1a [†]	DEM263	N157	Yes	LH100	PE	Yes	II
55	J053912.67-692941.4	2	DEM269	N158C	Yes	LH101	–	–	–
56	J053943.82-693834.0	2/3b+2/1a ^{†,*}	DEM284	N160A	Yes	LH103	Unknown	No	–
57	J054841.29-700536.7	2	DEM323	N180B	Yes	LH117	–	–	II/III
YSOs in H II regions									
58	J045426.06-691102.3	3a	DEM22	N83B	Yes	LH5	PE	No	III
59	J045708.84-662325.1	3a	DEM34	N11A	Yes	LH10	–	–	III
60	J045716.25-662319.9	3a	DEM34	N11	Yes	LH10	PE	No	II/III
61	J052207.27-675819.7	3a	DEM152	N44C	Yes	LH47	PE	No	II/III
62	J053845.15-690507.9	3a	DEM263	N157	Yes	LH100	PE	No	III
63	J053943.26-693854.6	3a	DEM284	N160A	Yes	LH103	Unknown	No	III
64	J053945.94-693839.2	3a	DEM284	N160A	Yes	LH103	Unknown	No	II/III
65	J054004.40-694437.6	3a	DEM271	N159B	Yes	LH105	PE	No	III
66	J052212.24-675813.1	3b	DEM152	N44C	Yes	LH47	–	–	–
67	J052249.13-680129.1	3b	DEM160	N44H	Yes	LH49	PE	No	II/III
68	J045429.42-690936.9	3c	DEM22	N83	Yes	LH5	–	–	II
69	J045651.82-663133.0	3c	DEM34	N11F	No	LH9	PE	No	II
70	J045720.72-662814.4	3c	DEM34	N11	No	–	PE	No	II/III
71	J053549.28-660133.5	3c	DEM243	N63	No	LH83	–	–	–
72	J053821.10-690617.2	3c	DEM263	N157	Yes	–	–	–	III
73	J053855.56-690426.5	3c	DEM263	N157	Yes	LH100	–	–	III
74	J053858.42-690434.7	3c	DEM263	N157	Yes	LH100	PE	No	III
75	J054844.29-700360.0	3c	DEM323	N180B	Yes	LH117	–	–	II/III
76	J054853.64-700320.2	3c	DEM323	N180B	Yes	LH117	–	–	II/III

^aThe identifier of the YSO shows the J2000 coordinates of the YSOs in *hhmmss.s-ddmmss.s* format.

^bCategory describes YSO environments: YSOs found in dark clouds without optical counterparts in *HST* H α images are 1a, YSOs in dark clouds with optical counterparts are 1b; YSOs in bright rimmed dust pillars are 2; YSOs with resolved H II regions are 3a, YSOs with marginally resolved H II regions are 3b, and YSOs with unresolved H II regions are 3c.

[†]YSOs are found in more than one kind of environment, e.g. 2/3b refers to YSOs which are associated with bright-rimmed dust

pillars and the optical counterpart is a small H II region.

*More than one YSOs is discovered in the *Spitzer* PSF.

Table 2. Properties of Resolved H II Regions Associated with Massive YSOs

ID	Length ^a (pc)	H α Flux ^b (ergs cm ⁻² s ⁻¹)	EM (cm ⁻⁶ pc)	n_e (cm ⁻³)	$L_{H\alpha}$ ^b (ergs s ⁻¹)	$Q(H_0)$ (photons s ⁻¹)	Sp.Type	IRS Spectra
J045426.06-691102.3	0.96	6.84×10^{-12}	2.86×10^5	546	1.45×10^{35}	1.03×10^{47}	B0.5	PE
J045708.84-662325.1	1.80	2.55×10^{-12}	7.59×10^3	64	5.40×10^{34}	3.94×10^{46}	B0.5	–
J045716.25-662319.9	1.68	8.64×10^{-12}	1.18×10^5	265	1.83×10^{35}	1.35×10^{47}	B0.5	PE
J052207.27-675819.7	0.33	3.19×10^{-14}	1.08×10^4	181	6.76×10^{32}	4.80×10^{44}	B2	PE
J053845.15-690507.9	0.81	2.38×10^{-12}	1.37×10^5	412	5.04×10^{34}	3.59×10^{46}	B0.5	PE
J053943.26-693854.6	0.96	7.92×10^{-12}	3.33×10^5	587	1.67×10^{35}	1.19×10^{47}	B0	Unknown
J053945.94-693839.2	1.44	1.07×10^{-11}	1.98×10^5	371	2.26×10^{35}	1.61×10^{47}	B0	Unknown
J054004.40-694437.6	0.96	2.78×10^{-12}	1.16×10^5	348	5.89×10^{34}	4.20×10^{46}	B0.5	PE

^aAverage emitting path lengths of the H II regions.

^bNot corrected for extinction.

Table 3. Properties of Marginally Resolved and Unresolved H II Regions Associated with Massive YSOs

ID	Category	Observed H α Flux (ergs cm $^{-2}$ s $^{-1}$)	Expected Cont. Flux ^a (ergs cm $^{-2}$ s $^{-1}$)	IRS Spectra
J052212.24-675813.1	3b	5.1×10^{-15}	1.3×10^{-15}	–
J052249.13-680129.1	3b	1.3×10^{-15}	–	PE
J053838.36-690630.4	3b	3.1×10^{-13}	6.7×10^{-14}	–
J053943.80-693834.0	3b	3.0×10^{-13}	–	Unknown
J045651.82-663133.0	3c	2.4×10^{-14}	1.8×10^{-14}	PE
J045429.42-690936.9	3c	1.1×10^{-13}	–	–
J045720.72-662814.4	3c	6.7×10^{-15}	1.1×10^{-14}	PE
J053549.28-660133.5	3c	7.0×10^{-15}	5.0×10^{-15}	–
J053609.54-691805.5	3c	4.4×10^{-14}	1.0×10^{-14}	–
J053821.10-690617.2	3c	3.1×10^{-14}	–	–
J053855.56-690426.5	3c	9.3×10^{-15}	1.0×10^{-14}	–
J053858.42-690434.7	3c	8.9×10^{-15}	9.7×10^{-15}	PE
J054844.29-700360.0	3c	6.6×10^{-15}	–	–
J054853.64-700320.2	3c	3.4×10^{-14}	4.0×10^{-15}	–

^aExpected continuum flux of the YSO in the H α passband.

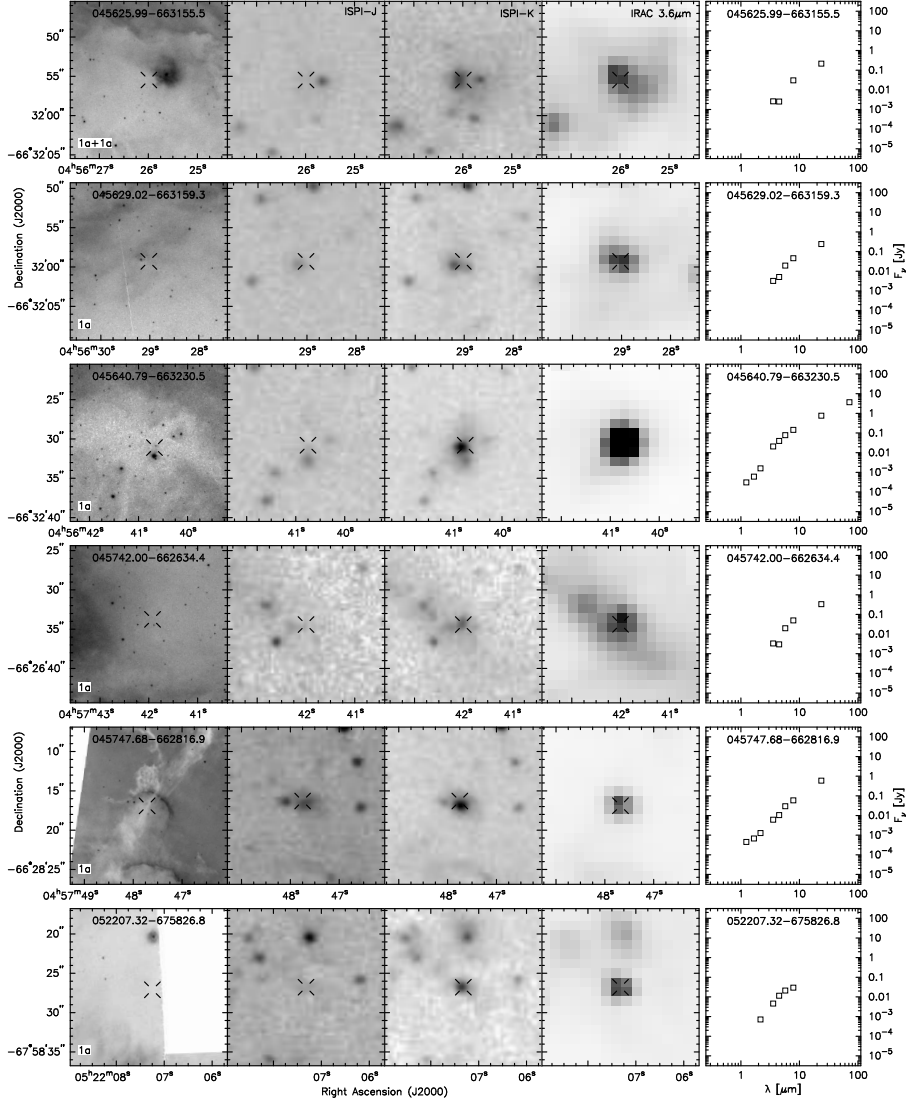
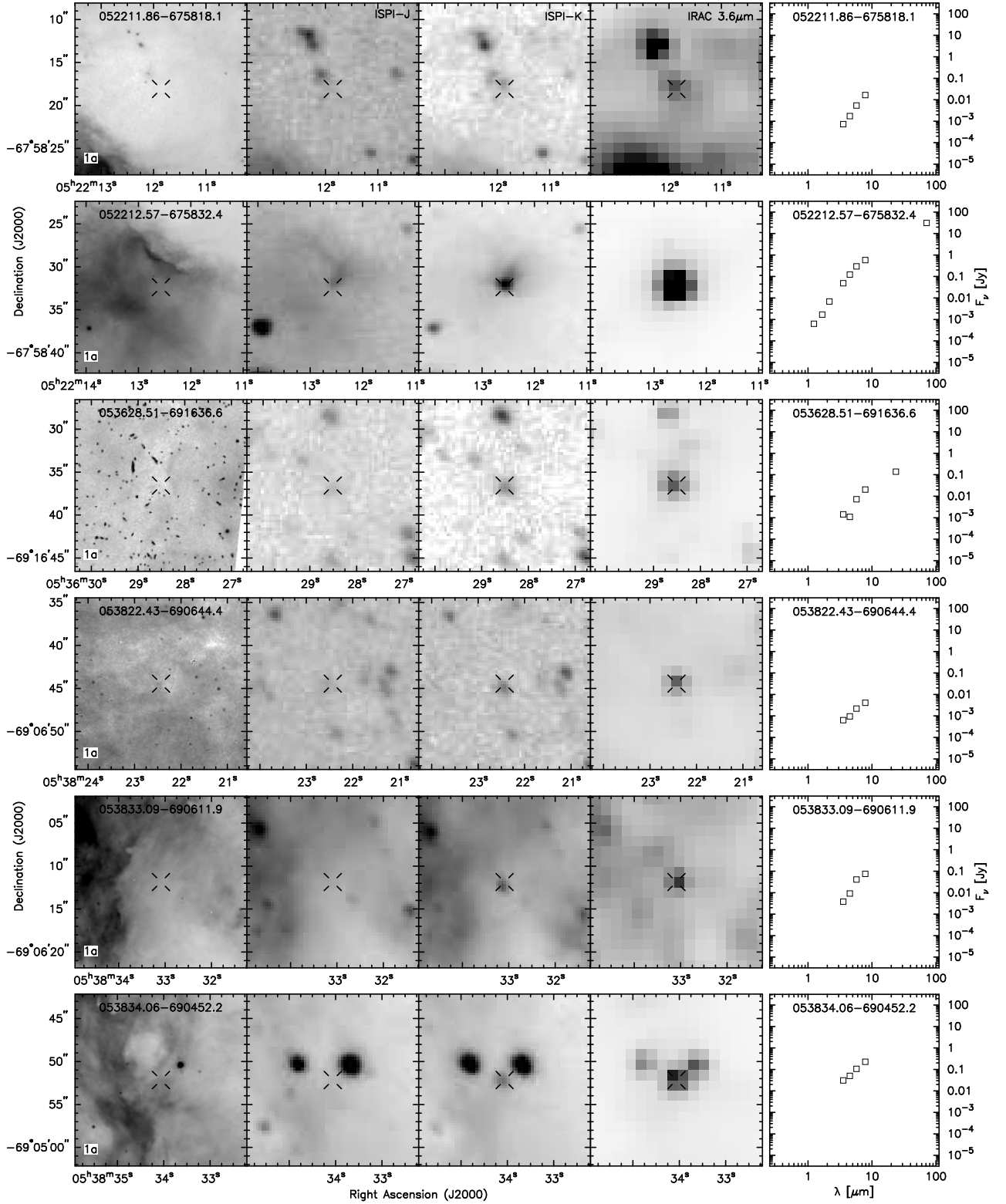
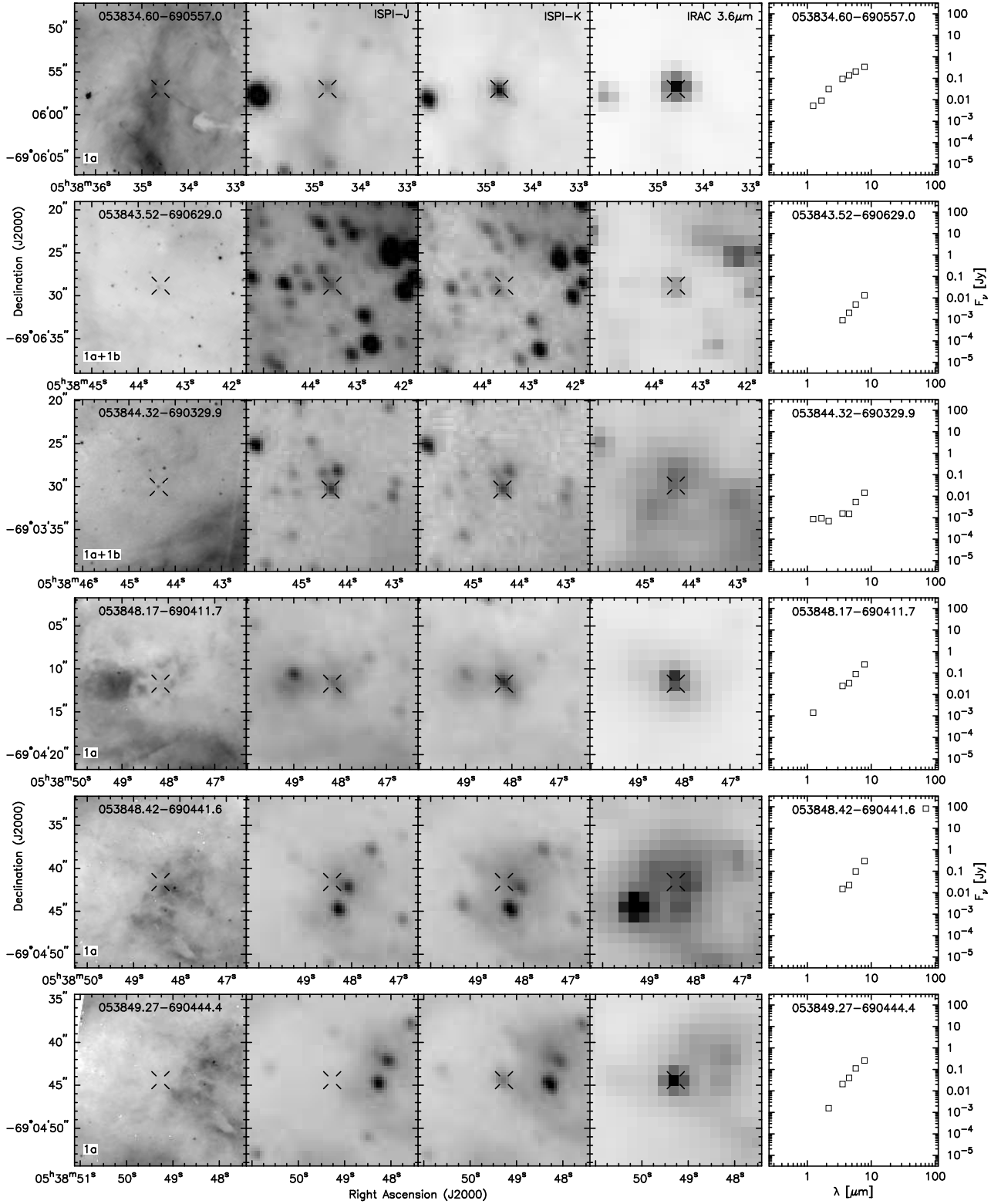
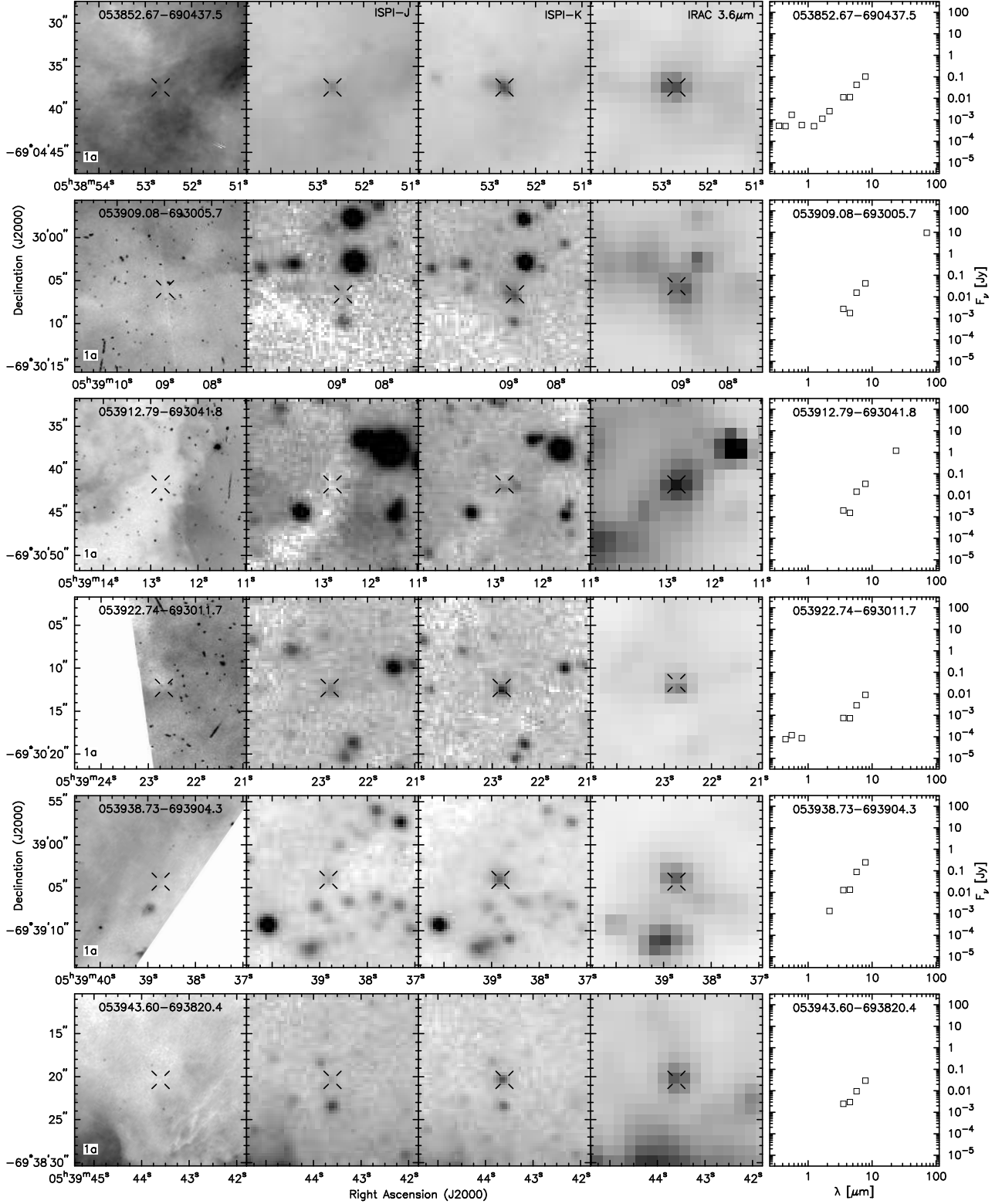
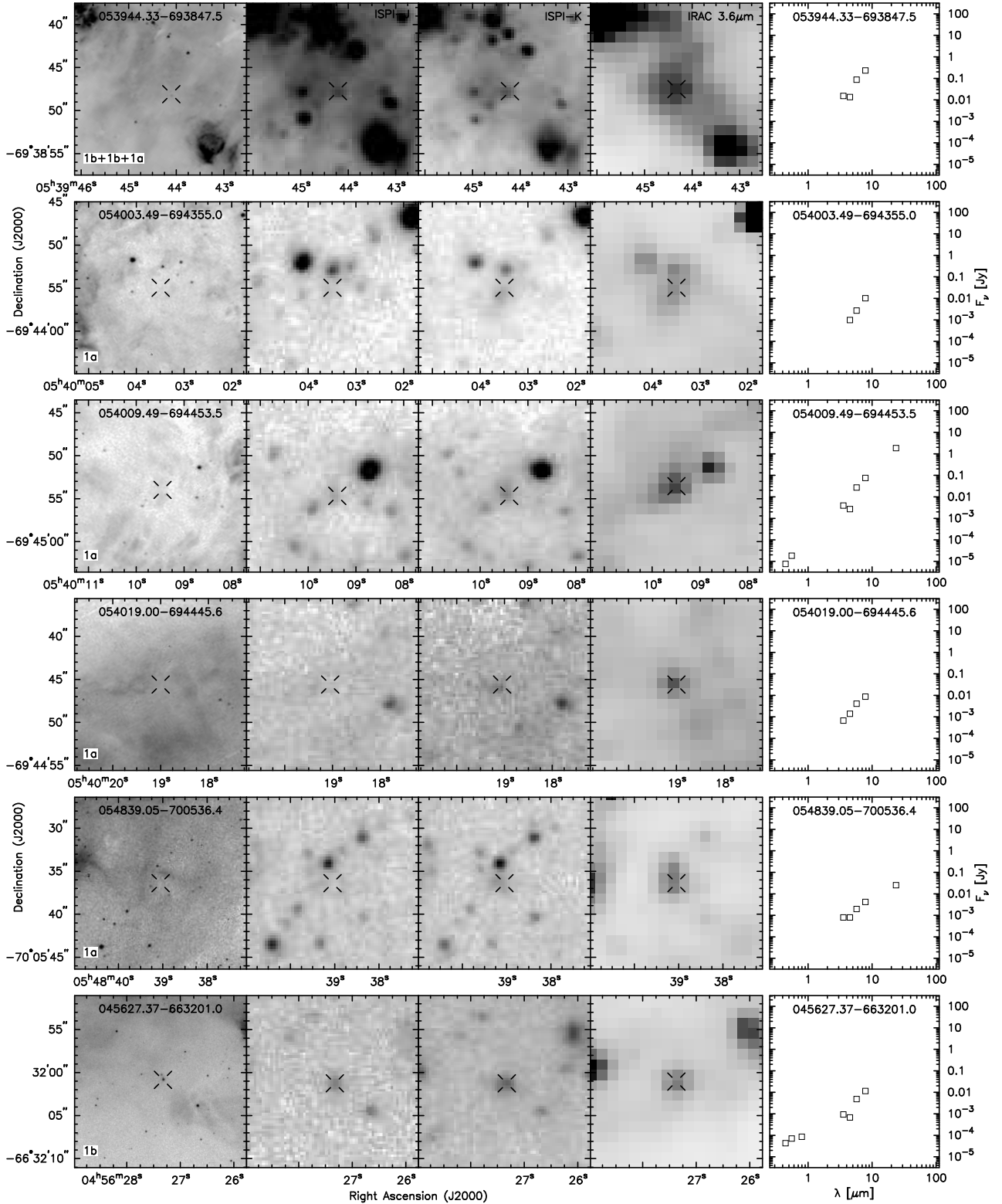


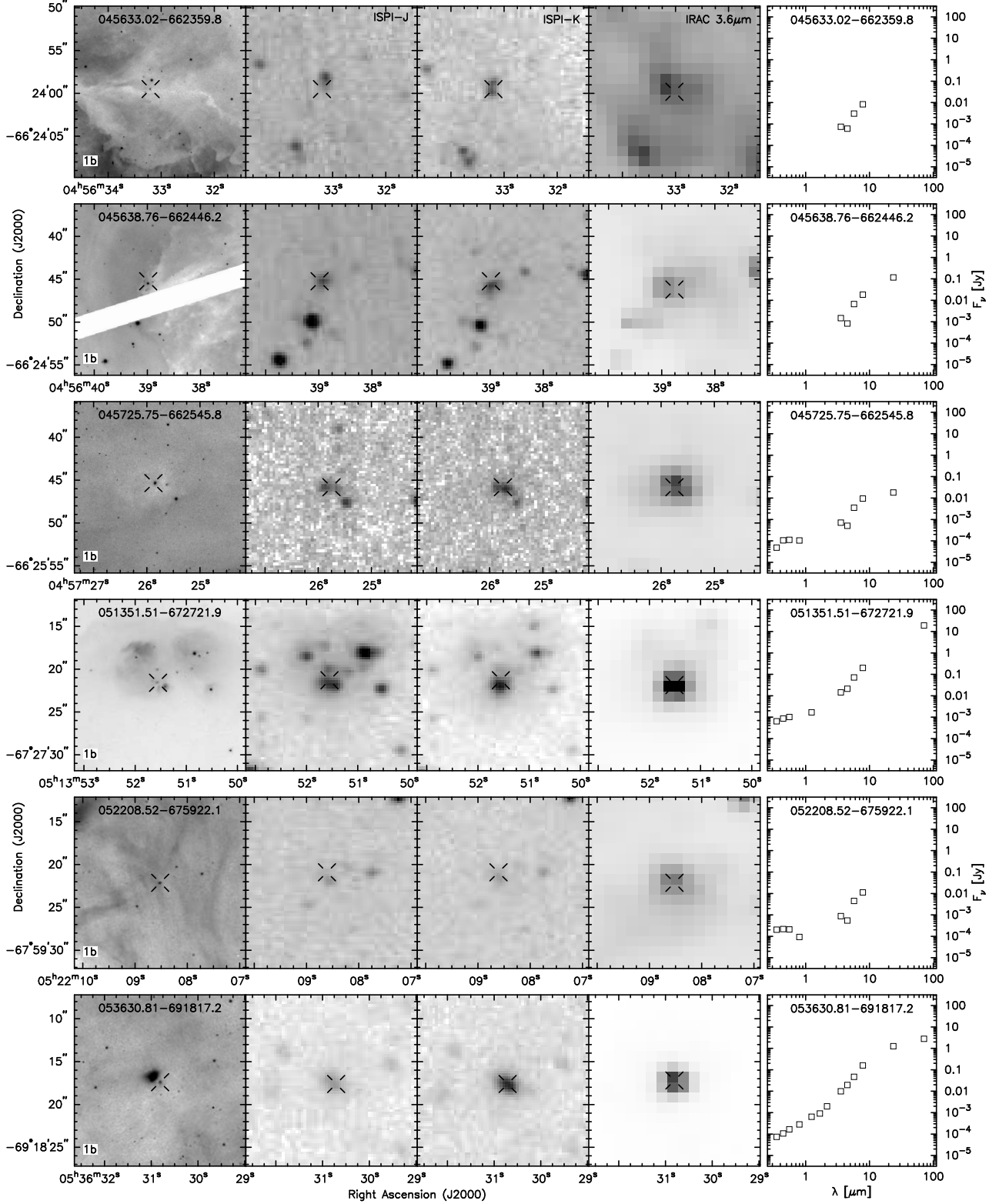
Fig. 1.— From left to right each set of five panels show $20'' \times 20''$ *HST* $H\alpha$, ISPI J , K_s , and *Spitzer* $3.6 \mu\text{m}$ images centered on the *Spitzer* position for each YSO, and the SED of the YSO. The position of the YSO and its optical near-IR counterparts are indicated with an open cross. The category for each YSO is indicated in the lower left corner where: YSOs in dark clouds without and with optical counterparts are marked as categories 1a and 1b, respectively; YSOs in bright-rimmed dust pillars are marked as category 2; YSOs associated with well-resolved, marginally resolved, and unresolved H II regions are marked as categories 3a, 3b, and 3c, respectively. Cases where multiple optical/near-IR counterparts are discovered within the *Spitzer* PSF are indicated with a “+” and YSOs found in more than one kind of environment are indicated with a “/”.

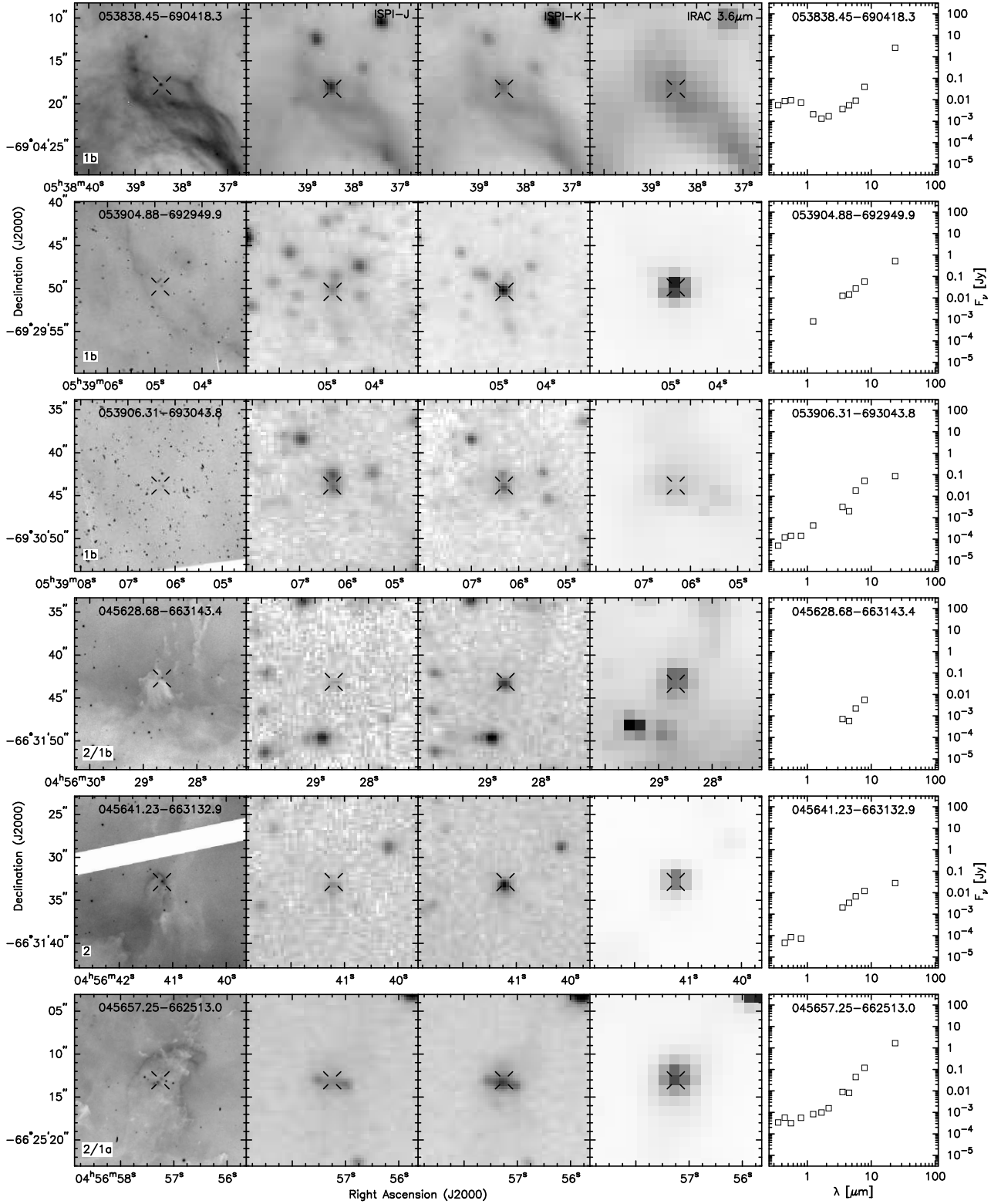


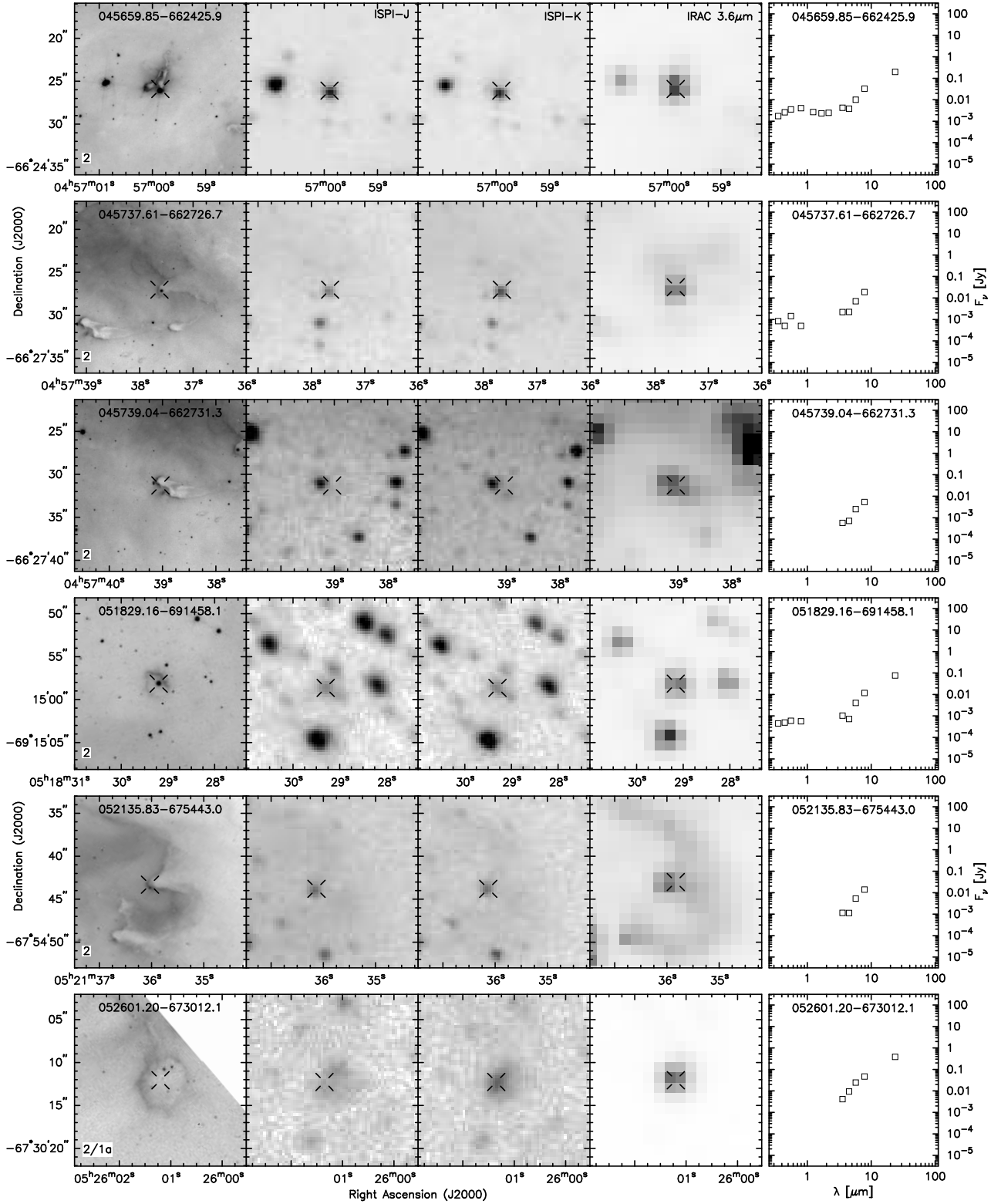


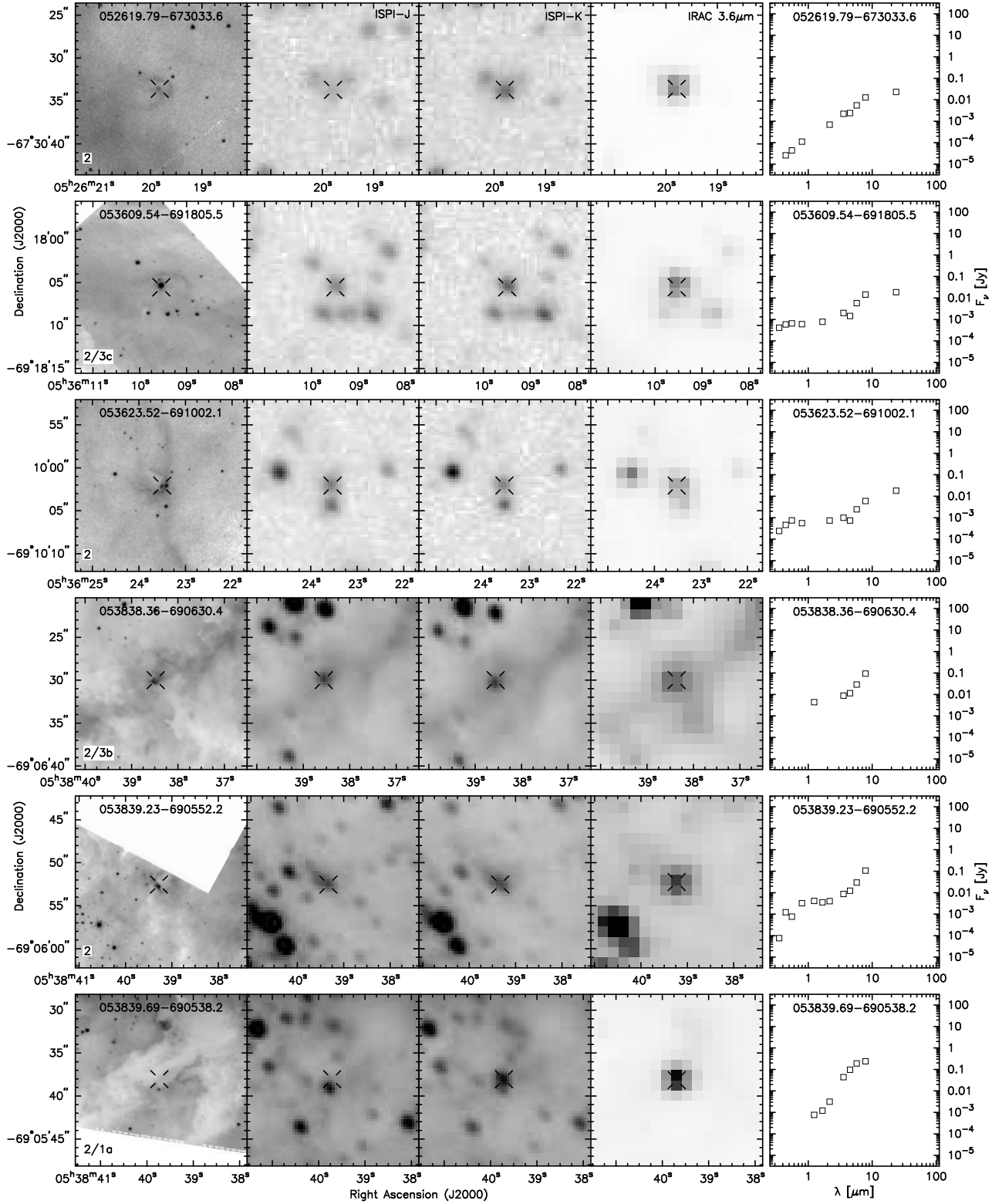


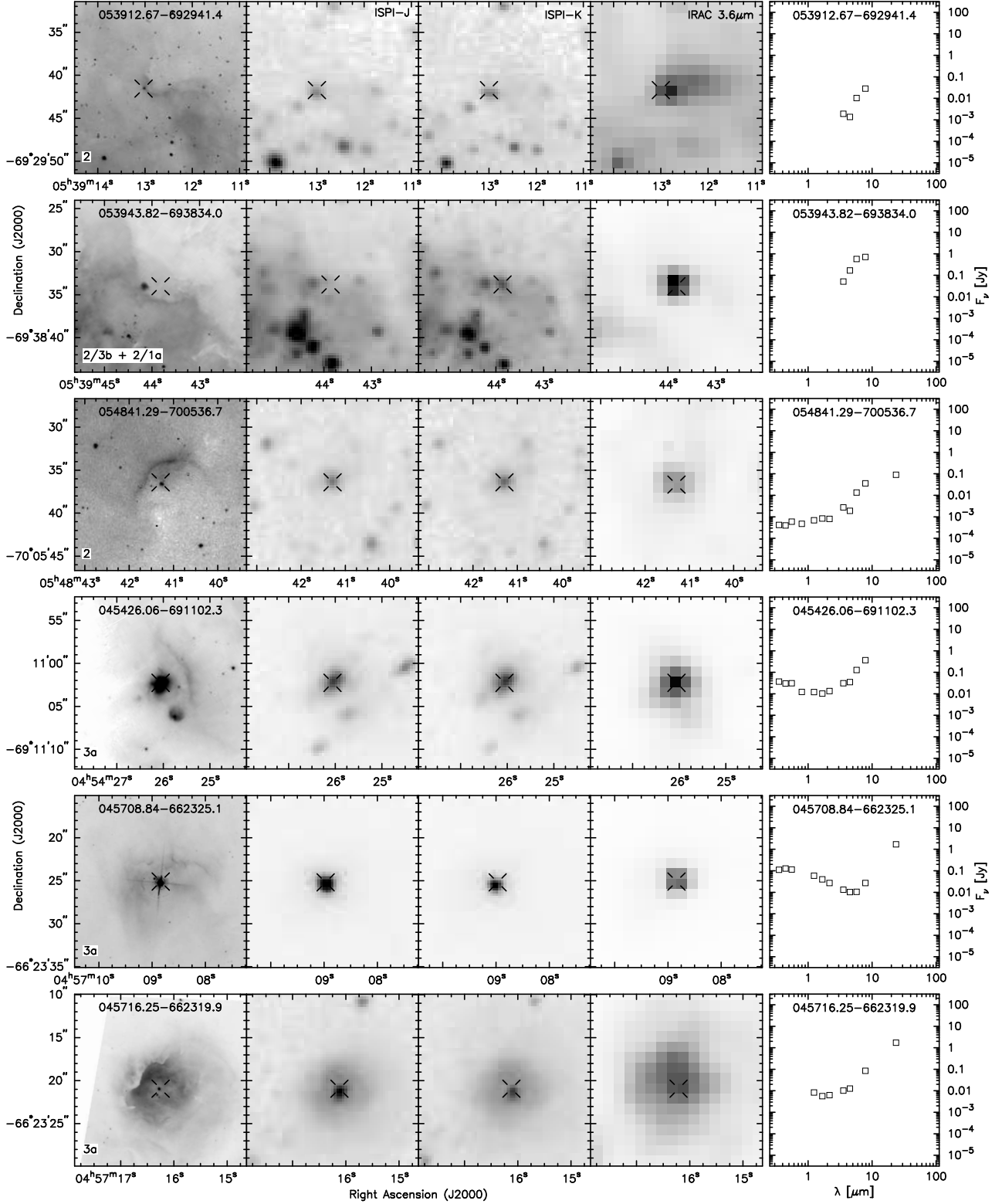


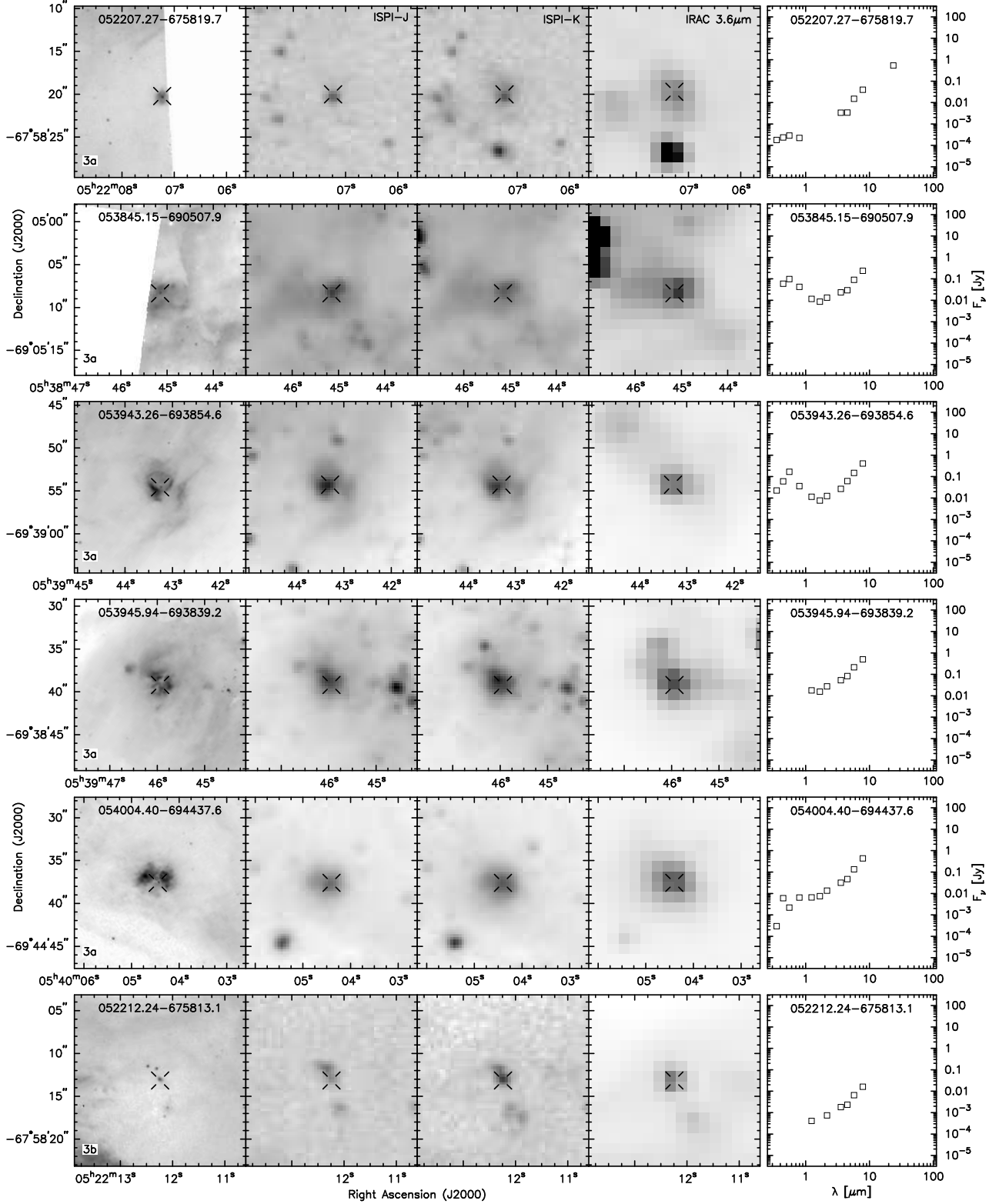


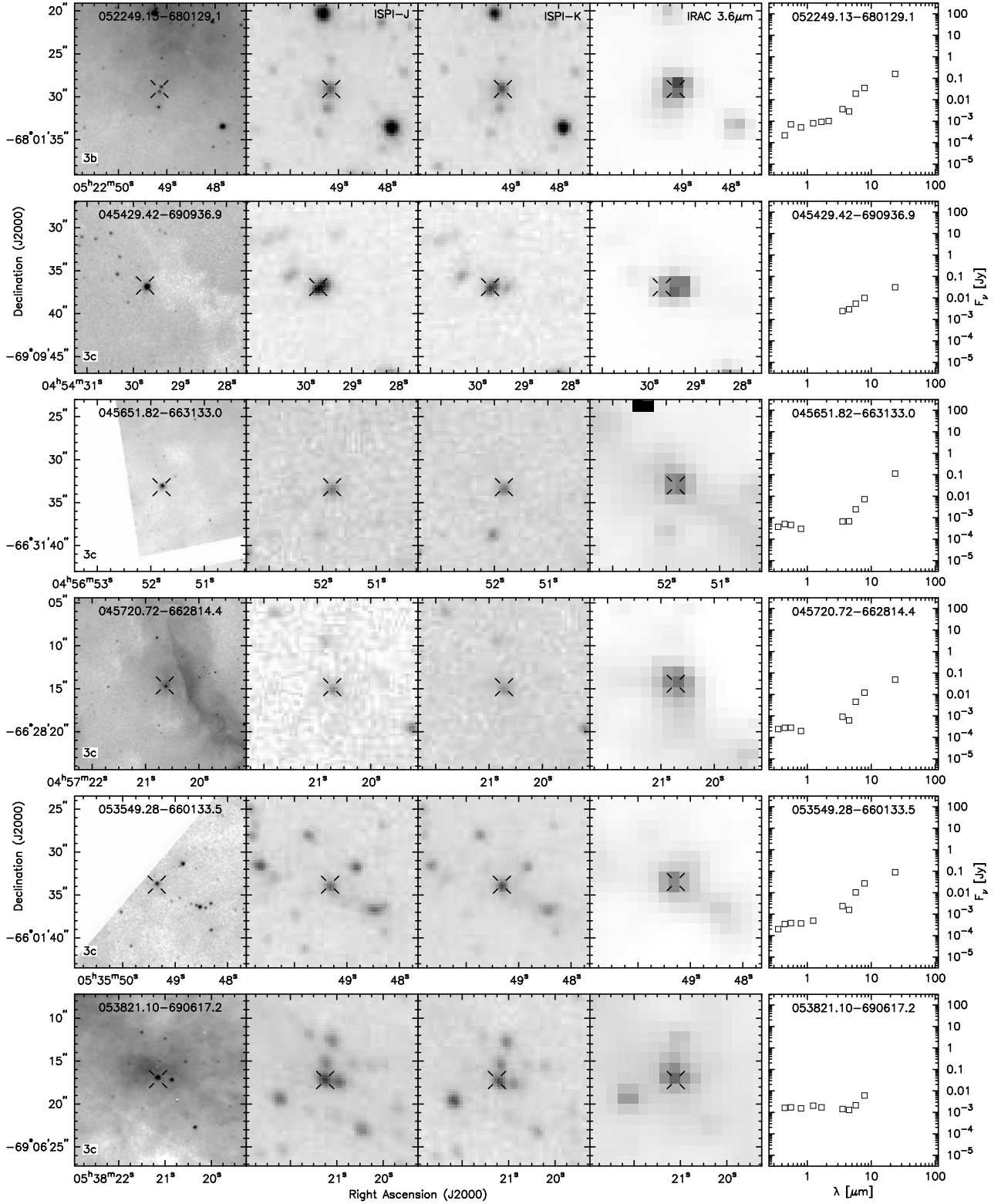


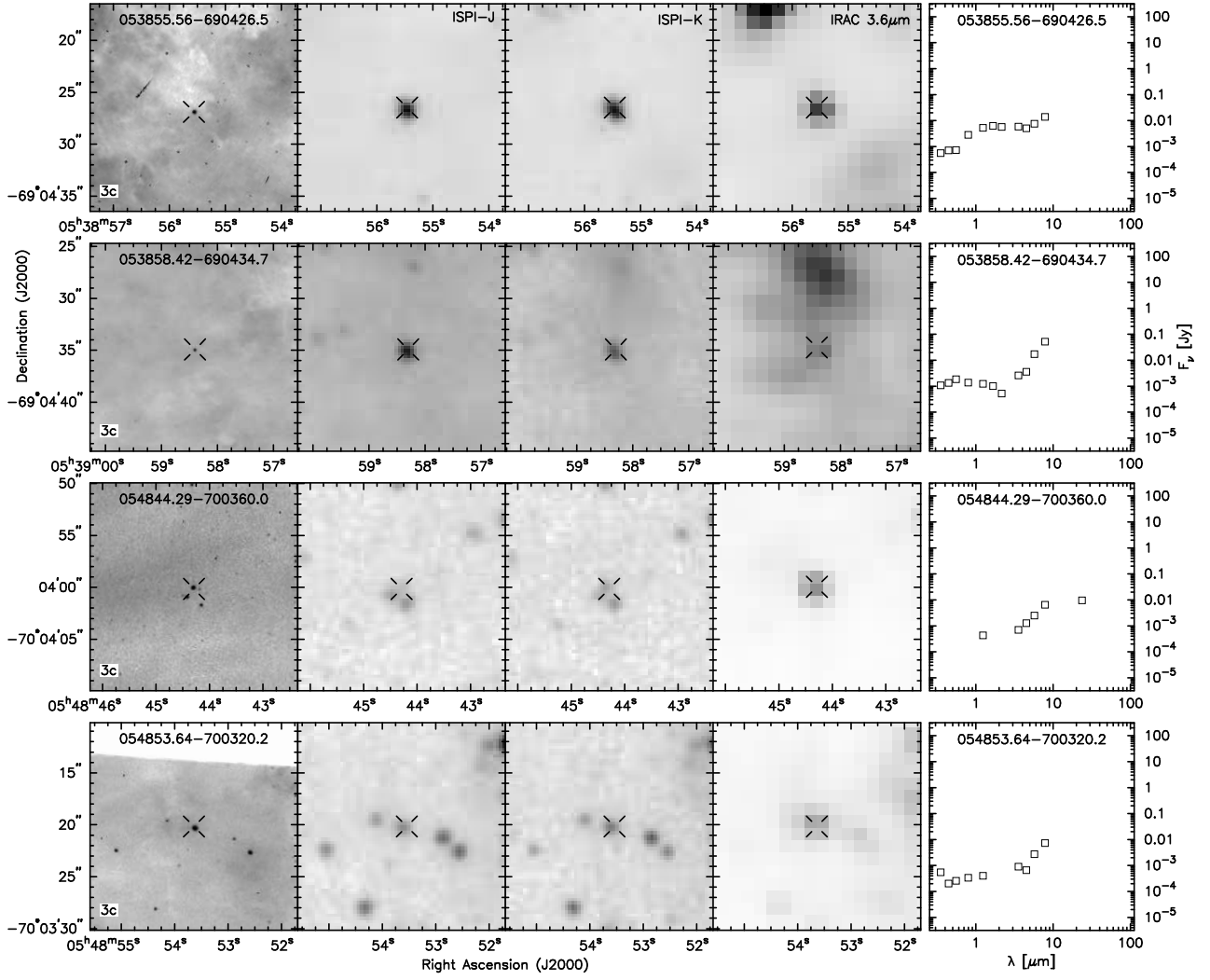












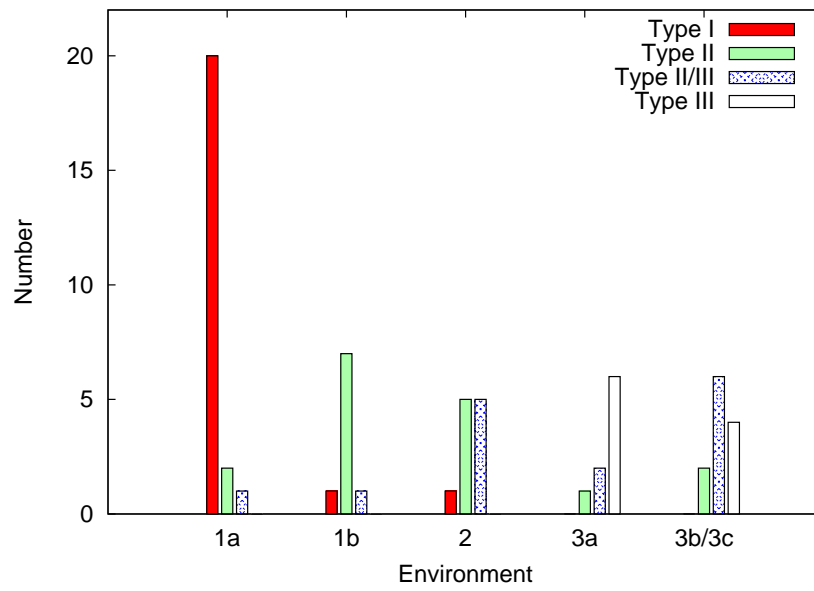


Fig. 2.— A histogram plot showing the correlation of YSO environments and the SED Type classification. YSOs in dark clouds with no optical counterparts are 1a, YSOs in dark clouds with optical counterparts are 1b, YSOs in bright rimmed dust globules are 2, YSOs with resolved H II regions are 3a, YSOs with marginally resolved H II regions are 3b and YSOs with unresolved H II regions are 3c.

Table 4. List of non-YSOs

Number	ID	Description
1	J045647.11-662459.1	Diffuse emission
2	J045658.24-662430.7	Diffuse emission
3	J045702.52-662503.3	Diffuse emission
4	J045726.42-662248.4	galaxy
5	J052218.80-675814.6	Diffuse emission
6	J053525.90-691428.6	galaxy
7	J053550.40-692422.0	galaxy
8	J053554.84-691426.6	Diffuse emission
9	J053627.62-691434.9	Diffuse emission
10	J053708.79-690720.3	A bright star
11	J053742.63-690943.6	Diffuse emission
12	J053825.21-690405.2	Diffuse emission
13	J053844.32-690329.9	Diffuse emission with perhaps faint YSOs
14	J053845.99-690930.8	Diffuse emission
15	J053848.86-690828.0	galaxy
16	J053906.22-692930.9	Star on diffuse emission
17	J053949.18-693747.4	Two galaxies